Interlayer transport of an electron in bilayer graphene with phonon-induced lattice distortion in the presence of biased potential*

He Liang-Ming(何良明)†

College of Science, Guangxi University for Nationalities, Nanning 530006, China

(Received 10 April 2012; revised manuscript received 28 June 2012)

The interlayer transport of an electron in bilayer graphene influenced by a phonon in the presence of a biased potential is investigated using the tight-binding approach. The in-plane optical mode E_{2g} and out-of-plane optical mode B_{1g} associated with the applied biased potential are considered to compute and discuss the interlayer transport probability of an electron initially localized on the bottom layer at the Dirac point in the Brillouin zone. Without the biased potential, the interlayer transport probability is equal to 0.5 regardless of the phonon displacement except for a few special cases. Applying a biased potential to the layers, we find that in different phonon modes the function of the transport probability with respect to the applied biased potential and phonon displacement is complex and various, but on the whole the transport probability decreases with the increase in the absolute value of the applied biased potential. These phenomena are discussed in detail in this paper.

Keywords: electronic transport, conductivity of specific materials

PACS: 72.10.Di, 72.80.–r **DOI:** 10.1088/1674-1056/22/1/017201

1. Introduction

Monolayer graphene and bilayer graphene have become the most animated areas of research because of their novel properties and potential applications in devices. Thus the electronic transport properties of monolayer graphene have been extensively studied.[1–4] However one of the major challenges in graphene-based electronics is that the conduction cannot be simply switched off by means of gate voltages because of the lack of a bandgap,[5] so it cannot be used as a logic gate to manipulate information. However, the bilayer graphene offers a solution to this problem with a gate tunable bandgap due to its interlayer hopping or by control with a gate voltage.[6–8] Recently, many researchers have paid attention to the electronic structures and transport properties of the bilayer graphene, such as hopping-resolved electron–phonon coupling,[9,10] electron screening and excitonic condensation,[11] correlation effects of Cooper pairing of electrons and holes,[12] and quantum Hall effect in the presence of disorder.[13] The electron–phonon interactions play an important role in the interaction between nearest neighbor atom orbits, thereby modulating the nearest neighbor hopping.[14,15] Based on the tight-binding models, the roles of the phonon in electronic band structures of monolayer graphene and bilayer graphene near the Dirac points were studied by Cappelluti *et al.*[10] They evaluated quantitatively the electron–phonon coupling associated with each hopping using different optical phonon displacements within the context of density functional theory. The energy splittings of the Dirac point, which depend on the phonon displacements, in the in-plane and the out-of-plane phonon modes were explored respectively. It is well known that in a monolayer graphene, the low-energy band is gapless and the electronic states are found near two Dirac cones. Near them the intralayer transport behavior of charge carriers (electrons and holes) has been studied by using the Dirac equation.[16–18] But for the bilayer graphene, the research work on the interlayer transport behavior, for which the Dirac equation is unavailable, has been rarely reported. In the present paper, we investigate the interlayer transport of the bilayer graphene with a lattice distortion induced respectively by the in-plane and the out-of-plane phonon modes.

2. Model

As described in Ref. [10], the hoppings in the tight-binding model of a bilayer graphene with the typical Bernal stacking are stipulated: γ_0 denotes the nearest neighbor in-plane hopping, γ_1 denotes the nearest neighbor vertical hopping, γ_3 denotes the hopping between atoms A1 and B2, and γ_4 describes the hopping between atom couples A1–A2 and B1–B2 (see Fig. 1). The magnitudes of these hoppings are ruled by the relative distances of the corresponding atoms, thus their modulations induced by the lattice displacement determine the electron–phonon interaction. From the viewpoint of energy, the electron–phonon interaction is equipollent to a deformation potential, which recomposes the system's Hamiltonian. In the frozen-phonon approach[19] and with the linear supposition of hoppings depending on the lattice distortion, the difference $\Delta\gamma_i$ of hopping γ_i due to the lattice distortion is proportional to the displacement per atom u, that is, $\Delta\gamma_i \propto u$. As shown Fig. 1, there are E_{2g} and B_{1g} optical phonon modes with lat-

*Project supported by the Department of Education of Guangxi, China (Grant No. 200911MS78).

†Corresponding author. E-mail: hlm66225@sohu.com

© 2013 Chinese Physical Society and IOP Publishing Ltd

tice wavevector $\boldsymbol{q}=0$. In these cases, there are relative movements between atoms A and B. In the monolayer graphene, E_{2g} and B_{1g} stand for in-plane and out-of-plane vibrations, respectively. For convenience, the in-plane modes E_{2g1} and E_{2g2} are chosen along x and y directions with $\boldsymbol{u}_{A1,x}=u_x\boldsymbol{x}^0$ and $\boldsymbol{u}_{A1,y}=u_y\boldsymbol{y}^0$, while the out-of-plane mode B_{1g} is along the z axis with $\boldsymbol{u}_{A1,z}=u_z\boldsymbol{z}^0$. The displacements of the other atoms are thus univocally determined by the components of the wavevector of the phonon mode.

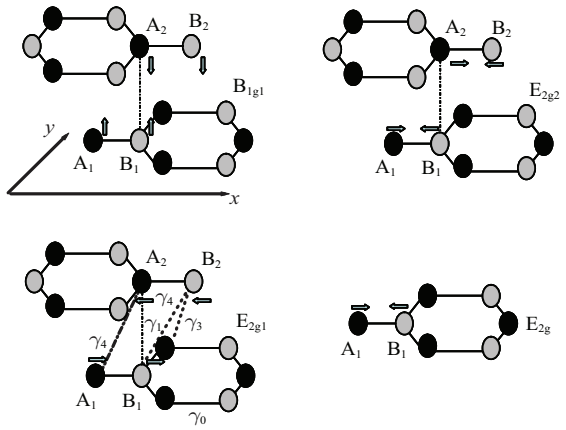


Fig. 1. Sketches of hoppings for bilayer graphene with the typical Bernal stacking and atomic displacements for the relevant phonon lattice modes B_{1g} and E_{2g}.

Based on the Bloch sums of $\boldsymbol{k}$ wavevector of monolayer graphene built from $2p_z$ orbitals of carbon atoms A and B in the unit cell, $\Phi_{Aj}(\boldsymbol{k})$ and $\Phi_{Bj}(\boldsymbol{k})$ ($j=1,2$; where $j=1$ stands for the bottom layer, and $j=2$ for the top layer), the low-energy Hamiltonian of the bilayer graphene with the typical Bernal stacking in the absence of lattice distortion reads

$$\boldsymbol{H}_0=\begin{pmatrix} U & \gamma_0 f_{\boldsymbol{k}} & \gamma_4 f_{\boldsymbol{k}} & \gamma_3 f_{\boldsymbol{k}}^* \\ \gamma_0 f_{\boldsymbol{k}}^* & \delta+U & \gamma_1 & \gamma_4 f_{\boldsymbol{k}} \\ \gamma_4 f_{\boldsymbol{k}}^* & \gamma_1 & \delta & \gamma_0 f_{\boldsymbol{k}} \\ \gamma_3 f_{\boldsymbol{k}} & \gamma_4 f_{\boldsymbol{k}}^* & \gamma_0 f_{\boldsymbol{k}}^* & 0 \end{pmatrix}, \tag{1}$$

where $f_{\boldsymbol{k}}=\mathrm{e}^{-\mathrm{i}k_x a/\sqrt{3}}+2\mathrm{e}^{\mathrm{i}k_x a/2\sqrt{3}}\cos(k_y a/2)$, and δ is the difference of the crystal field probed by B1–A2 carbon atoms in the bilayer structure with respect to A1–B2 atoms, which is assumed not to be changed by the phonon for being tiny. The U is a biased potential applied between the two layers (the top with potential U and the bottom without potential). Introducing the phonon-induced distortion to such a bilayer, the Hamiltonian involved the deformation potential determined by the electron–phonon interaction becomes[10]

$$\boldsymbol{H}=\boldsymbol{H}_0+u_i\begin{pmatrix} 0 & \beta_{\boldsymbol{k}}(12) & \beta_{\boldsymbol{k}}(13) & \beta_{\boldsymbol{k}}(14) \\ \beta_{\boldsymbol{k}}(12)^* & 0 & \beta_{\boldsymbol{k}}(23) & \beta_{\boldsymbol{k}}(24) \\ \beta_{\boldsymbol{k}}(13)^* & \beta_{\boldsymbol{k}}(23)^* & 0 & \beta_{\boldsymbol{k}}(34) \\ \beta_{\boldsymbol{k}}(14)^* & \beta_{\boldsymbol{k}}(24)^* & \beta_{\boldsymbol{k}}(34)^* & 0 \end{pmatrix}, \tag{2}$$

where $i=1,2,3$ denote x, y, z directions, respectively, the parameters $\{\beta_{\boldsymbol{k}}\}$ are coefficients for linearly determining the difference $\Delta\gamma_j$ of hopping γ_j in terms of $\Delta\gamma_j\propto u_i$, which are illuminated as follows. (i) In the case of phonon mode B_{1g1} ($\boldsymbol{u}_{A1,z}=u_z\boldsymbol{z}^0$), $\beta_{\boldsymbol{k}}(23)=2\alpha_1$, the other $\beta_{\boldsymbol{k}}$ are naught. (ii) Under the E_{2g1} mode ($\boldsymbol{u}_{A1,x}=u_x\boldsymbol{x}^0$), $\beta_{\boldsymbol{k}}(12)=\beta_{\boldsymbol{k}}(23)=\beta_{\boldsymbol{k}}(34)=0$, $\beta_{\boldsymbol{k}}(13)=\beta_{\boldsymbol{k}}(24)=\alpha_4 g_{\boldsymbol{k}}\cos\theta$, $\beta_{\boldsymbol{k}}(14)=-\alpha_3 g_{\boldsymbol{k}}^*\cos\theta$. (iii) For E_{2g2} mode along the x direction ($\boldsymbol{u}_{A1,x}=u_x\boldsymbol{x}^0$), $\beta_{\boldsymbol{k}}(13)=\beta_{\boldsymbol{k}}(23)=\beta_{\boldsymbol{k}}(24)=0$, $\beta_{\boldsymbol{k}}(12)=\beta_{\boldsymbol{k}}(34)=\alpha_0 g_{\boldsymbol{k}}$, $\beta_{\boldsymbol{k}}(14)=-\alpha_3 g_{\boldsymbol{k}}^*\cos\theta$. (iv) For E_{2g2} mode along the y direction ($\boldsymbol{u}_{A1,y}=u_y\boldsymbol{y}^0$), $\beta_{\boldsymbol{k}}(13)=\beta_{\boldsymbol{k}}(23)=\beta_{\boldsymbol{k}}(24)=0$, $\beta_{\boldsymbol{k}}(12)=\beta_{\boldsymbol{k}}(34)=\alpha_0 h_{\boldsymbol{k}}$, $\beta_{\boldsymbol{k}}(14)=\alpha_3 h_{\boldsymbol{k}}^*\cos\theta$. Here, $g_{\boldsymbol{k}}=2\mathrm{e}^{-\mathrm{i}k_x a/\sqrt{3}}-2\mathrm{e}^{\mathrm{i}k_x a/2\sqrt{3}}\cos(k_y a/2)$, $h_{\boldsymbol{k}}=\mathrm{i}2\sqrt{3}\mathrm{e}^{\mathrm{i}k_x a/2\sqrt{3}}\sin(k_y a/2)$, and $\cos\theta$ is a geometric factor accounting for the projection of the lattice displacement along the direction of the γ_3 hopping bond. The α_0, α_1, α_3, and α_4 are electron–phonon couplings corresponding to hoppings γ_0, γ_1, γ_3, and γ_4, respectively.

In dealing with the movement of an electron in molecules or solid matters, the vibrations of molecules or atoms are frozen since they are much slower than the movement of electrons. This is called the frozen-phonon approach. In this approach, by diagonalizing the Hamiltonian $\boldsymbol{H}$ given in expression (2), the system's exact eigenvalue $\xi_l(\boldsymbol{k})$ and eigenvector $\psi_l(\boldsymbol{k})$ can be obtained, therefore the exact evolving state $\Psi(\boldsymbol{k},t)$ originating from an arbitrary initial state $\Psi(\boldsymbol{k},0)=a\Phi_{A1}(\boldsymbol{k})+b\Phi_{B1}(\boldsymbol{k})$, where $a^2+b^2=1$, is obtained as $\Psi(\boldsymbol{k},t)=\sum_l\langle\psi_l(\boldsymbol{k})|\Psi(\boldsymbol{k},0)\rangle\exp(-\mathrm{i}\xi_l t/\hbar)|\psi_l(\boldsymbol{k})\rangle$. Consequently, the probability $P_{\mathrm{top}}(t)$, with which the electron initially localized on the bottom layer is found on the top layer at time t, is given by $P_{\mathrm{top}}(t)=[\sum_l\langle\psi_l(\boldsymbol{k})|\Psi(\boldsymbol{k},0)\rangle\exp(-\mathrm{i}\xi_l t/\hbar)\langle\Phi_{A2}(\boldsymbol{k})|\psi_l(\boldsymbol{k})\rangle]^2+[\sum_l\langle\psi_l(\boldsymbol{k})|\Psi(\boldsymbol{k},0)\rangle\exp(-\mathrm{i}\xi_l t/\hbar)\langle\Phi_{B2}(\boldsymbol{k})|\psi_2(\boldsymbol{k})\rangle]^2$, and thus the averaged probability over time t is

$$P_{\mathrm{top}}=\sum_l(\langle\psi_l(\boldsymbol{k})|\Psi(\boldsymbol{k},0)\rangle)^2(\langle\Phi_{A2}(\boldsymbol{k})|\psi_l(\boldsymbol{k})\rangle)^2+\sum_l(\langle\psi_l(\boldsymbol{k})|\Psi(\boldsymbol{k},0)\rangle)^2(\langle\Phi_{B2}(\boldsymbol{k})|\psi_2(\boldsymbol{k})\rangle)^2. \tag{3}$$

Using Eq. (3), we can study the interlayer transport probability of an electron initially localized at the bottom layer with wavevector $\boldsymbol{k}$ by numeral simulation.

3. Simulation and discussion

For an isolated monolayer graphene, K-point (i.e., Dirac point) in the Brillouin zone is at the Fermi surface. Therefore the electronic conductivity and optical property of the monolayer graphene are closely correlated with electrons near the Dirac point. The point $\boldsymbol{k}=(2\pi a)(0,2/3)$ is one of the Dirac points. Without loss of universality, here we investigate the interlayer transport of an electron at this Dirac point in the Brillouin zone from the bottom to the top with initial state $\Psi(t=0)=\Phi_{A1}$ or $\Psi(t=0)=\Phi_{B1}$. In this case, $f_{\boldsymbol{k}}=0$, $h_{\boldsymbol{k}}=3\mathrm{i}$, and $g_{\boldsymbol{k}}=3$ in expression (2). Note that all parameters for simulations are taken from Ref. [10], specialized as follows: $\gamma_1=-0.35$ eV, $\delta=-0.0119$ eV, $\alpha_0=-4.41$ eV/Å,

$\alpha_1 = -0.68$ eV/Å, $\alpha_3 = -0.54$ eV/Å, $\alpha_4 = -0.32$ eV/Å, and $\cos\theta = 0.39$. To study the dependence of interlayer transport of an electron on the applied potential U and the displacement per atom u, we chose u from the interval [–0.05 Å, 0.05 Å] and U from [–2 eV, 2 eV].

The influence of B_{1g} mode phonon is considered first. In this case, all carbon atoms vibrate vertically to the plane of graphene along the z direction, and the Hamiltonian is

$$\boldsymbol{H} = \begin{pmatrix} U & 0 & 0 & 0 \\ 0 & U+\delta & \gamma_1+2\alpha_1 u_z & 0 \\ 0 & \gamma_1+2\alpha_1 u_z & \delta & 0 \\ 0 & 0 & 0 & 0 \end{pmatrix}. \tag{4}$$

From expression (4), we know that the electron located initially at the bottom layer with initial state $\Psi(t=0) = \Phi_{A1}$ does not transport to the top layer, since the wavefunction Φ_{A1} does not mix with the system's eigenvectors and thus the term $\langle \psi_l \mid \Psi(0)\rangle = 0$ in expression (3). For the electron with initial state $\Psi(t=0) = \Phi_{B1}$, Fig. 2 shows its interlayer transport probability from the bottom to the top as a function of the displacement per atom u_z and the applied biased potential U. The function is approximately linear, i.e., roughly, P_{top} depends linearly on u_z for a fixed U, and for a given P_{top} there approximately exists a linear relation between U and u_z. Figure 2 also reveals that the interlayer transport probabilities increase with the increase of u_z, while they decrease with the accretion in absolute value of the applied potential U. It can be theoretically analyzed. Based on the eigenvalues and eigenvectors of the Hamiltonian in expression (4), from Eq. (3), we have

$$P_{top} = 4(\gamma_1+2\alpha_1 u_z)^2 \left\{ \frac{(\Delta-U)^2}{[4(\gamma_1+2\alpha_1 u_z)^2+(\Delta-U)^2]^2} + \frac{(\Delta+U)^2}{[4(\gamma_1+2\alpha_1 u_z)^2+(\Delta+U)^2]^2} \right\}, \tag{5}$$

where $\Delta = \sqrt{U^2+4(\gamma_1+2\alpha_1 u_z)^2}$. Subsequently, $P_{top} \approx 0.5$ for $U \approx 0$; $P_{top} \approx 0.1(\gamma_1+2\alpha_1 u_z)^2/U^2$ for $U \approx \gamma_1$; and $P_{top} \approx (\gamma_1+2\alpha_1 u_z)^2/U^2$ for $U \gg \gamma_1$. Therefore, $\pm U\sqrt{10P_{top}} \approx \gamma_1+2\alpha_1 u_z$ for $U \approx \gamma_1$ and $\pm U\sqrt{P_{top}} \approx \gamma_1+2\alpha_1 u_z$ for $U \gg \gamma_1$. As exhibited in the inset of Fig. 1, this is consistent with the linear relation of U and u_z, and the changes of slope can be interpreted as well. For a given U (with $U \gg \gamma_1$ or $U \approx \gamma_1$), $P_{top} \propto (\gamma_1+2\alpha_1 u_z)^2/U^2 \approx \gamma_1^2/U^2 + 4\alpha_1\gamma_1 u_z/U^2$, which explains the function of P_{top} with respect to u_z for a given U.

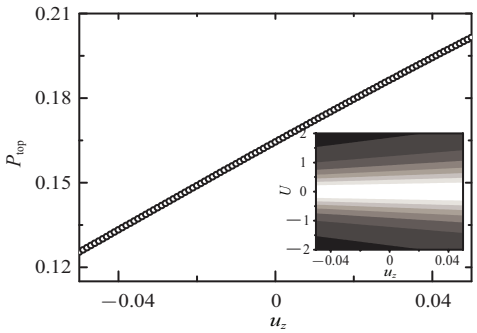


Fig. 2. Interlayer transport probability P_{top} as a function of applied biased potential U and displacement per atom u_z for an electron at initial state $\Psi(t=0) = \Phi_{B1}$. In the inset, P_{top} is scaled in gray, and deep gray corresponds to tiny probability. The circles give P_{top} versus u_z at $U = -1.0$ eV.

In E_{2g2} phonon mode, atoms vibrate in the plane of graphene. The Hamiltonians of a system with E_{2g2} phonon along x and y directions respectively are

$$\boldsymbol{H} = \begin{pmatrix} U & 3\alpha_0 u_x & 0 & -3\alpha_3 u_x\cos\theta \\ 3\alpha_0 u_x & U+\delta & \gamma_1 & 0 \\ 0 & \gamma_1 & \delta & 3\alpha_0 u_x \\ -3\alpha_3 u_x\cos\theta & 0 & 3\alpha_0 u_x & 0 \end{pmatrix}, \tag{6}$$

and

$$\boldsymbol{H} = \begin{pmatrix} U & -\mathrm{i}3\alpha_0 u_y & 0 & -\mathrm{i}3\alpha_3 u_y\cos\theta \\ \mathrm{i}3\alpha_0 u_y & U+\delta & \gamma_1 & 0 \\ 0 & \gamma_1 & \delta & -\mathrm{i}3\alpha_0 u_y \\ \mathrm{i}3\alpha_3 u_y\cos\theta & 0 & \mathrm{i}3\alpha_0 u_y & 0 \end{pmatrix}. \tag{7}$$

Figure 3 shows P_{top} as a function of displacement per atom and applied potential in these two cases for an electron with initial state $\Psi(t=0) = \Phi_{A1}$ and $\Psi(t=0) = \Phi_{B1}$, respectively, where P_{top} is maximum (about 0.5) when U and u_x (u_y) near the point (0, 0), but at which $P_{top} = 0$ when $\Psi(t=0) = \Phi_{A1}$. This results from the Hamiltonian

$$\boldsymbol{H} = \begin{pmatrix} 0 & 0 & 0 & 0 \\ 0 & \delta & \gamma_1 & 0 \\ 0 & \gamma_1 & \delta & 0 \\ 0 & 0 & 0 & 0 \end{pmatrix}. \tag{8}$$

As mentioned above, here the electron with initial state $\Psi(t=0) = \Phi_{A1}$ does not transport to the top layer since Φ_{A1} does not mix with the eigenvectors of Hamiltonian H. For $\Psi(t=0) = \Phi_{B1}$, it is easily obtained $P_{top} = 0.5$ from expressions (3) and (8). For $U \gg 0$ and $u_x(u_y) \approx 0$, we have $P_{top} \approx \gamma_1^2/U^2$ based on expressions (3) and (7). This makes it clear why P_{top} in Fig. 3 is tiny when $U \gg 0$ and $u_x(u_y) \approx 0$. Figure 3 shows that P_{top} decreases with the increase of $|U|$ although its dependence on U and $u_x(u_y)$ is variable. Similar to the discovery in Ref. [10], the symmetry in E_{2g2} mode along the y direction is also found by comparing carefully Fig. 3(c) with Fig. 3(d), i.e., unlike the displacements along x, P_{top} is symmetric with respect to $u_y \to -u_y$.

Finally, we consider the influence of E_{2g1} phonon mode associated with the applied potential on the interlayer transport. In this case, the Hamiltonian $\boldsymbol{H}$ with the phonon along the x direction is

$$\boldsymbol{H} = \begin{pmatrix} U & 0 & 3\alpha_4 u_x\cos\theta & -3\alpha_3 u_x\cos\theta \\ 0 & \delta+U & \gamma_1 & 3\alpha_4 u_x\cos\theta \\ 3\alpha_4 u_x\cos\theta & \gamma_1 & \delta & 0 \\ -3\alpha_3 u_x\cos\theta & 3\alpha_4 u_x\cos\theta & 0 & 0 \end{pmatrix}. \tag{9}$$

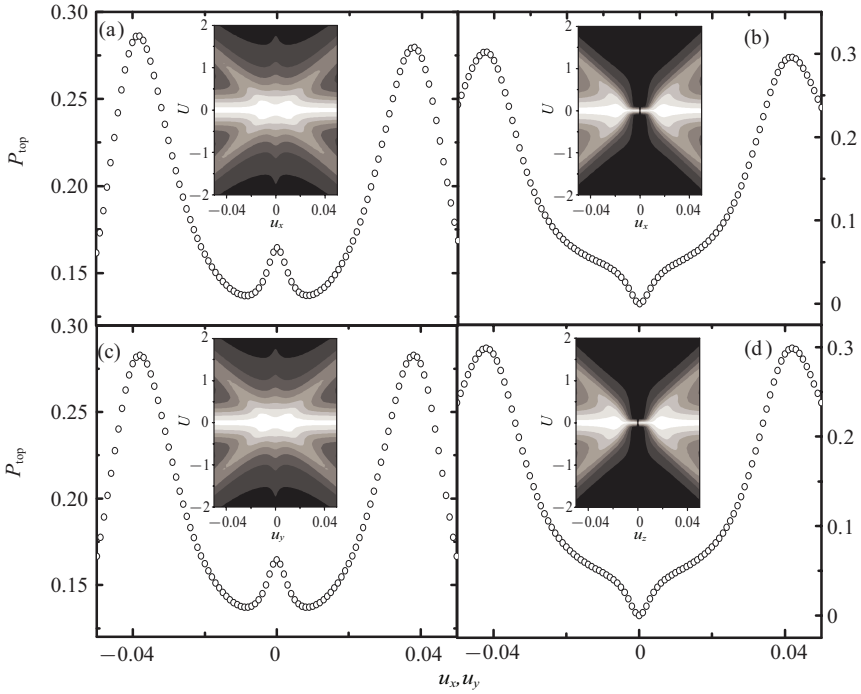


Fig. 3. The P_{top} as a function of displacement per atom and applied potential in the E_{2g2} mode along x and y directions, respectively: (a) for x direction with $\Psi(t=0)=\Phi_{B1}$, (b) for x direction with $\Psi(t=0)=\Phi_{A1}$, (c) for y direction with $\Psi(t=0)=\Phi_{B1}$, (d) for y direction with $\Psi(t=0)=\Phi_{A1}$. The circles give P_{top} versus $u_x(u_y)$ at $U=-1.0$ eV.

The P_{top} as a function of U and u_x is plotted in Figs. 4 and 5, which illuminate that it reduces with the accretion of U, and reduces much more quickly in Fig. 5. In addition, P_{top} changes very little with the displacement u_x when $\Psi(t=0)=\Phi_{B1}$, while for $\Psi(t=0)=\Phi_{A1}$, P_{top} is also found equal to naught at the point ($U=0$, $u_x=0$). To analyze theoretically these phenomena, we rewrite the Hamiltonian as $\boldsymbol{H}=\boldsymbol{H}^0+\boldsymbol{H}'$ and assume $U \gg \gamma_1$, where

$$\boldsymbol{H}^0=\begin{pmatrix} U & 0 & 0 & 0 \\ 0 & U+\delta & 0 & 0 \\ 0 & 0 & \delta & 0 \\ 0 & 0 & 0 & 0 \end{pmatrix}, \tag{10}$$

and $\boldsymbol{H}'$ are considered to be a perturbation on $\boldsymbol{H}^0$, with

$$\boldsymbol{H}'=\begin{pmatrix} 0 & 0 & 3\alpha_4 u_x\cos\theta & -3\alpha_3 u_x\cos\theta \\ 0 & \delta & \gamma_1 & 3\alpha_4 u_x\cos\theta \\ 3\alpha_4 u_x\cos\theta & \gamma_1 & \delta & 0 \\ -3\alpha_3 u_x\cos\theta & 3\alpha_4 u_x\cos\theta & 0 & 0 \end{pmatrix}. \tag{11}$$

We know that γ_1 is much larger than the other matrix elements in expression (11). In terms of the first-order perturbation theory, the wavevector Φ_{B1} mixes into the eigenvectors of $\boldsymbol{H}$ with probabilities $(3\alpha_4 u_x\cos\theta/(U-\delta))^2$ and $(\gamma_1/U)^2$, while the wavevector Φ_{B1} mixes with probabilities $(3\alpha_3 u_x\cos\theta/U)^2$ and $(3\alpha_4 u_x\cos\theta/(U+\delta))^2$ into the eigenvectors of $\boldsymbol{H}$. In the case of $\Psi(t=0)=\Phi_{B1}$, the interlayer transport probability P_{top} in expression (3) is dominated by $(\gamma_1/U)^2$ since it is much larger than $(3\alpha_4 u_x\cos\theta/(U-\delta))^2$.

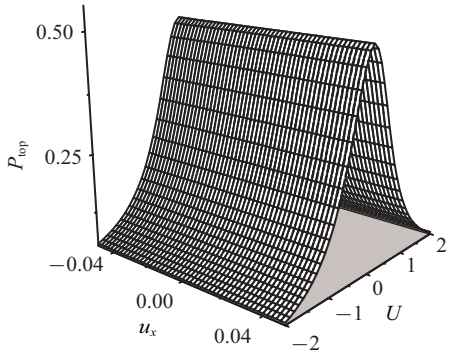


Fig. 4. The P_{top} as a function of displacement per atom and applied potential in the E_{2g1} mode along the x direction with initial state $\Psi(t=0)=\Phi_{B1}$.

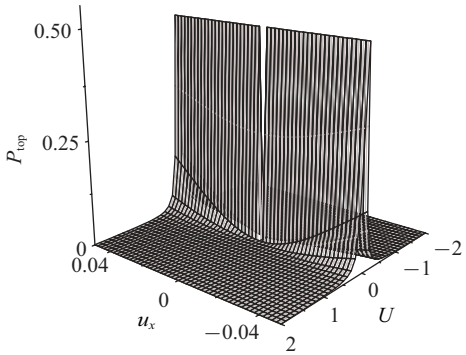


Fig. 5. The P_{top} as a function of displacement per atom and applied potential in the E_{2g1} mode along the x direction with initial state $\Psi(t=0)=\Phi_{A1}$.

This is why $P_{\rm top}$ changes mainly depend on U regardless of the change of u_x in Fig. 4. At the same time, it explains why $P_{\rm top}$ reduces much more quickly with U when $\Psi(t=0)=\Phi_{\rm A1}$ than when $\Psi(t=0)=\Phi_{\rm B1}$. For $P_{\rm top}=0$ at point (0, 0) when $\Psi(t=0)=\Phi_{\rm A1}$, the explanation is the same as that for Figs. 3(b) and 3(d). It is noted that similar to the E_{2g2} mode along the y direction, $P_{\rm top}$ of the E_{2g1} mode along the y direction is very like that along the x direction, except for the symmetry ($u_y \to -u_y$) in the E_{2g1} mode along the y direction.

4. Conclusion

In this paper, we have studied the electronic interlayer transport of bilayer graphene, which is influenced by a phonon and applied biased potential. For a Dirac electron, the interlayer transport probability is banal with value of 0.5 or 0 regardless of phonon's movement. When a biased potential is applied to the bilayer graphene, the dependence of the transport probability on phonon is rich and various. We find that the biased potential weakens the effect of the phonon on the interlayer transport probability, that is, it decreases with the increase of the absolute value of the biased potential. It is noted that these results hold for electrons with wavevector $\boldsymbol{k}$ very near the Dirac point. As mentioned in the above sections, the phonon not only works on the electronic interlayer transport but also splits the Dirac cone, and consequently influences the electronic intralayer transport. The biased potential or biased voltage as a gate applied on the bilayer graphene thus can control the interlayer transport as well as the intralayer transport. In this sense, our results associated with the detailed theoretical analysis are useful for understanding the graphene-based electronics.

References

[1] McCann E and Falko V I 2006 *Phys. Rev. Lett.* **96** 086805
[2] Checkelsky J G, Li L and Ong N P 2008 *Phys. Rev. Lett.* **100** 206801
[3] Hasegawa Y and Kohmoto M 2006 *Phys. Rev.* B **74** 155415
[4] Xu X G, Zhang C, Xu G J and Cao J C 2011 *Chin. Phys.* B **20** 27201
[5] CastroNeto A H, CastroNeto, Guinea F, Peres N M R, Novoselov K S and Geim A K 2009 *Rev. Mod. Phys.* **81** 109
[6] Allen M T, Martin J and Yacoby A 2012 *Nature Commun.* **3** 934
[7] Zhang Y, Tang T T, Girit C, Hao Z, Martin M C, Zettl A, Crommie M F, Shen Y R and Wang F 2009 *Nature* **459** 820
[8] Mak K F, Lui C H, Shan J and Heinz T F 2009 *Phys. Rev. Lett.* **102** 256405
[9] Ochoa H, Castro E V, Katsnelson M I and Guinea F 2011 *Phys. Rev.* B **83** 235416
[10] Cappelluti E and Profeta G 2012 *Phys. Rev.* B **85** 205436
[11] Min H, Bistritzer R, Su J J and MacDonald A H 2008 *Phys. Rev.* B **78** 121401(R)
[12] Eisenstein J P and MacDonald A H 2004 *Nature* **432** 691
[13] Novoselov K S, McCann E, Morozov S V, Fal'ko V I, Katsnelson M I, Zeitler U, Jiang D, Schedin F and Geim A K 2006 *Nature Phys.* **2** 177
[14] Mañes J L, Guinea F and Vozmediano M A H 2007 *Phys. Rev.* B **75** 155424
[15] Samsonidze Ge G, Barros E B, Saito R, Jiang J, Dresselhaus G and Dresselhaus M S 2007 *Phys. Rev.* B **75** 155420
[16] Slonczewski J C and Weiss P R 1958 *Phys. Rev.* **109** 272
[17] Semenoff G W 1984 *Phys. Rev. Lett.* **53** 2449
[18] Yury P B, Valentin F, Sergey S and Franco N 2009 *Phys. Rev.* B **79** 075123
[19] Khan F S and Allen P B 1984 *Phys. Rev.* B **29** 3341